Journal of Sound and Vibration 329 (2010) 4486–4500

Contents lists available at ScienceDirect

Journal of Sound and Vibration

journal homepage: www.elsevier.com/locate/jsvi

Dynamic analysis of clamp band joint system subjected to axial vibration

Z.Y. Qin, S.Z. Yan, F.L. Chu *

Department of Precision Instruments and Mechanology, Tsinghua University, Beijing 100084, China

ARTICLE INFO

Article history:
Received 8 November 2009
Received in revised form
22 April 2010
Accepted 14 May 2010
Handling Editor: L.G. Tham

ABSTRACT

Clamp band joints are commonly used for connecting circular components together in industry. Some of the systems jointed by clamp band are subjected to dynamic load. However, very little research on the dynamic characteristics for this kind of joint can be found in the literature. In this paper, a dynamic model for clamp band joint system is developed. Contact and frictional slip between the components are accommodated in this model. Nonlinear finite element analysis is conducted to identify the model parameters. Then static experiments are carried out on a scaled model of the clamp band joint to validate the joint model. Finally, the model is adopted to study the dynamic characteristics of the clamp band joint system subjected to axial harmonic excitation and the effects of the wedge angle of the clamp band joint and the preload on the response. The model proposed in this paper can represent the nonlinearity of the clamp band joint and be used conveniently to investigate the effects of the structural and loading parameters on the dynamic characteristics of this type of joint system.

1. Introduction

Clamp band joints are widely used for connecting components such as flanges, pipes and other shell segments. They can offer the joint systems with the properties of simple configuration and reliable operation. Another important application of clamp band is as a mechanical spacecraft attachment to launch vehicles in the aerospace industry. For different working conditions the configuration of clamp band joint varies slightly, while the working principle remains the same. Circumferential preload is applied on the clamp band during assembling to insure reliable connection. However, there exists slippage between the joint surfaces inevitably that leads to nonlinear stiffness and damping. In the exacting environment of spacecraft launching, these local nonlinearities would result in unpredictable behavior of the launch system during the launch and ascent period and even affect the success of launch event [1,2]. It is, therefore, vital to construct the dynamic model for clamp band joint and investigate the nonlinear dynamic characteristics of the joint system.

Much research on the modeling and dynamic analysis of the joint configuration had been carried out [3–6], most of which focused on the bolted joint and the discussions about clamp band joint were few. Robert and Michael [7] performed two full-scale structural tests and discussed the axial capability of the marman clamp using a nonlinear, axisymmetric finite element model. The analysis results showed that the gap capability of the marman clamp could be used to define the allowable clamp design load, which was increased by 50% compared with the allowable design load generated using conservative methods. Shoghi et al. [8,9] calculated the stress distribution and displacements of the V-section band clamp

* Corresponding author. Tel.: +86 10 6279 2842; fax: +86 10 6278 8308.
E-mail address: chufl@mail.tsinghua.edu.cn (F.L. Chu).

0022-460X/$ - see front matter © 2010 Elsevier Ltd. All rights reserved.
doi:10.1016/j.jsv.2010.05.012

and the flat section band clamp. The results were validated by strain and displacement measurements. Qin et al. [10] constructed theoretical models for the clamp band joint to calculate the axial stiffness and discussed the effects of the magnitude of the preload on the system stiffness and load capability. It was indicated that the increment of the preload could improve the load capability of the clamp band joint but had a little effect on the joint stiffness. Although the works of these literatures are useful for the design and the assembling of the clamp band joint, all of them are limited to static analysis and the dynamic model of the clamp band joint is still not available.

In this paper, a dynamic model was developed to characterize the forced response of the clamp band joint system subjected to axial excitation. First, the axial motion equation for the flange of the interface ring jointed by clamp band was derived based on the analysis of the interaction and deformation of the clamp band components. Then the dynamic model for the clamp band joint system was developed, where contact and frictional slippage between V-segments and interface rings were considered. Nonlinear finite element analysis was carried out to identify contact parameters of the dynamic model. The joint model was verified by static experiments undertaken on a 1:2.5 scale clamp band joint model. Finally, the dynamic characteristics of the clamp band joint system under axial excitation were studied and the payload response was compared with that of the configuration having no relative displacement between the joint surfaces to investigate the nonlinearity presented by the clamp band joint. The effects of the wedge angle of the clamp band joint and the preload on the system responses were also discussed based on the proposed model.

2. Derivation of dynamic model for clamp band joint system

2.1. Assumptions

The configuration of the clamp band joint for fastening spacecraft to launch vehicle is shown in Fig. 1, in which the separation springs and the lateral springs are not illustrated since they have little effect on the joining behavior of the clamp band joint. The joint system consists of two half metal belts that are fastened together by bolts, V-segments and upper and lower interface rings. By tightening of the two bolts, the tension in the metal belts increases, which leads to the application of a circumferential force to the V-segments encircled by metal belts. Then the wedging action of the V-segments onto the flanges of the interface rings generates an axial load that can join the interface rings together and allow them to sustain applied tensile forces and bending moments.

Considering the configuration and assembly of the clamp band joint [10,11] assumptions are made in the derivation of the dynamic equations for clamp band joint system under preload and axial excitation as follows.

(1) All components of the clamp band joint system respond in a linear elastic manner.
(2) The magnitude of tension in the metal belts remains constant in a motion cycle, which is equal to the preload applied during assembling.
(3) Friction between the metal belts and the V-segments is ignored so that the tension in the belts and the contact force between the metal belts and the V-segments are uniformly distributed along the circumference.
(4) The distribution of V-segments is continuous along the circumference. Together with assumption (3), it can be derived that the joint system is under axisymmetric load condition and the deformations of interface rings in all radial sections are uniform. Hence, it is sufficient to consider deformations only in one radial section through the axis of symmetry.
(5) The deformations of upper and lower interface rings are symmetrical about the joint surface so that the tangential contact force on the joint surface is ignored.

2.2. Axial motion equation for flange of interface ring

The free-body diagram for a radial section of the upper interface ring and the upper portion of one V-segment is shown in Fig. 2, where the interface ring is sectioned into a cylindrical shell and a flange, and p_t, q_t and m_t are the internal forces and moment on the section. It should be noted that the forces and moment acting on the radial section of the interface ring

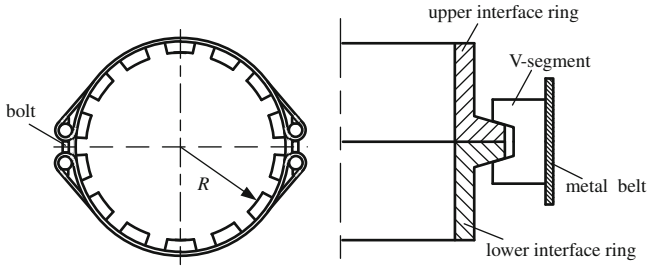

Fig. 1. Sketch of clamp band join.

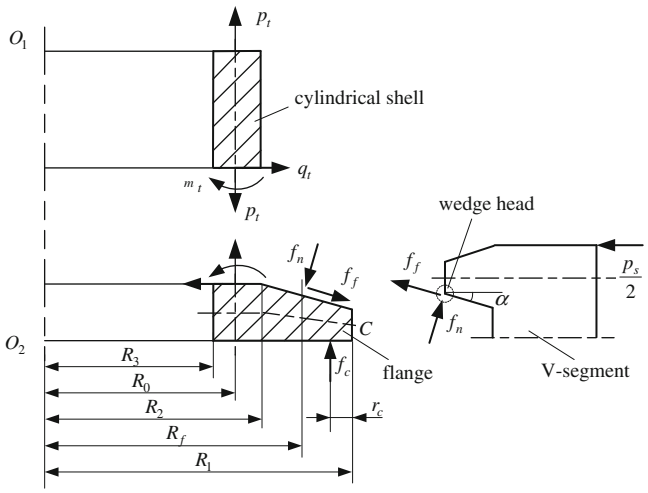

Fig. 2. Free-body diagram of upper frame and V-segment cross section.

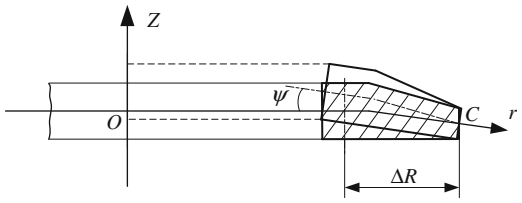

Fig. 3. Sketch of torsional deformation of the flange.

and the V-segment are distributed along their acting line. The forces and moment shown in Fig. 2 are resultants per unit length of the acting circumference. In addition, the distribution of those contact forces f_n, f_f and f_c varies along with the magnitude of the applied load and the deformation, which will be discussed in Section 3.

Considering that the cross-sectional dimensions of the flange are much small in comparison with the average radius, the bending deformation of the flange is neglected and the flange motion is then reduced to two degrees of freedom including torsion about point C on the outer edge and compression in radial direction. Only the torsional motion is considered here as illustrated in Fig. 3, where Z and r indicate the axial and radial directions, respectively, ψ denotes the flange rotation angle about the point C, $\Delta R=R_1-R_0$ is the radial distance from the middle surface of cylindrical shell to the rotational center C. Taking ψ as displacement coordinate, the torsional motion equation for the flange under the axial excitation can be obtained by using the Lagrange's equation

$$\rho I_p\ddot{\psi}+\frac{EI_r}{\overline{R}^2}\psi=\frac{M}{2\pi\overline{R}} \tag{1}$$

where ρ is the density of the ring material, $I_r=I_{r1}+I_{r2}$, $I_{r1}=\int_{R_3}^{R_2}\int_{-t_0/2}^{t_0/2}z^2\,dz\,dr$, $I_{r2}=\int_{R_2}^{R_1}\int_{-t_r/2}^{t_r/2}z^2\,dz\,dr$ are the mass moments of inertia of rectangular and trapezoid portions of the flange radial section, respectively, $I_p=I_{p1}+I_{p2}$, $I_{p1}=\int_{R_3}^{R_2}\int_{-t_0/2}^{t_0/2}\left[(R_1-r)^2+z^2\right]dz\,dr$, $I_{p2}=\int_{R_2}^{R_1}\int_{-t_r/2}^{t_r/2}[(R_1-r)^2+z^2]dz\,dr$ are the polar moments of inertia of rectangular and trapezoid portions of the flange radial section about the rotational center C, respectively, $\overline{R}=R_1+R_2/2$ is the average radius of the flange, M is the resultant moment of those forces and moment acting on the flange about the rotational center C, which is given by

$$M=2\pi\overline{R}\left[p_t(R_1-R_0)+f_cr_c-f_v(R_1-R_f)-f_h\frac{t_f}{2}-q_t\frac{t_0}{2}-m_t\right] \tag{2}$$

where p_t is the axial excitation applied to the interface ring per unit length of the circumference of cylindrical shell, f_v and f_h are axial and radial components of the contact force between the flange and the V-segment, respectively, f_c is the normal contact force between upper and lower rings, q_t and m_t are the internal shear force and bending moment on the section of the cylindrical shell and the flange, respectively, t_0 and $t_f=t_0-2(R_f-R_2)\tan(\alpha/2)$ are the flange thickness in the axial direction at the points where q_t and f_h are applied, respectively, R_f is the radius at the acting point of f_v and f_h, r_c is the radial distance from the acting point of f_c to the outer edge of the flange.

Expressions for m_t and q_t can be obtained by using the condition of deformation continuity at the shell-flange junction [12] as below

$$\begin{aligned} m_t &= \frac{Et_s}{2\beta^3 {R_0}^2}(\psi-\beta u)+\frac{v}{2\beta^2 R_0}p_t \\ q_t &= \frac{Et_s}{2\beta^2 {R_0}^2}(\psi-2\beta u)+\frac{v}{\beta R_0}p_t \end{aligned} \tag{3}$$

where $\beta=\sqrt[4]{3(1-v^2)/(R_0t_s)^2}$ is the attenuation coefficient, in which v is the Poisson's ratio of the interface ring material, and t_s the thickness of the cylindrical shell, u is the radial compression of the flange, which is induced by the tension in the metal belt and the radial constraint of the cylindrical shell and can be expressed as

$$u=\frac{(p_s+2q_t)\overline{R}^2}{2EA} \tag{4}$$

where p_s is the contact force between the metal belt and the V-segment induced by the preload per unit length of the circumference of metal belts, E is the elastic modulus of the interface ring material and A is the area of the interface ring cross section.

Considering the action of the external forces and the equilibrium equations of the components shown in Fig. 2, the following relations can be obtained:

$$\begin{aligned} p_t &= T/2\pi R_0 \\ p_s &= S/R_b \\ f_v &= f_n\cos\alpha+f_f\sin\alpha \\ f_h &= f_n\sin\alpha-f_f\cos\alpha=p_s/2 \\ f_c &= f_v-p_t \end{aligned} \tag{5}$$

where T is the applied axial load, S is the tension in the metal belts, f_n and f_f are the contact forces between the upper ring and the V-segment in normal and tangential directions, respectively, R_0 and R_b are the radii of the middle surfaces of the cylindrical shell and the metal belts respectively. Substituting Eqs. (3)–(5) into Eq. (2) yields

$$M=2\pi\overline{R}\left\{\left[(R_1-R_0-r_c)-\frac{vR_0A(\beta t_0+1)}{2\beta^2{R_0}^2A+2\beta\overline{R}^2t_s}\right]p_t-(R_1-R_f-r_c)f_v+\left[\frac{\overline{R}^2t_s(\beta t_0+1)}{2\beta^2{R_0}^2A+2\beta\overline{R}^2t_s}-\frac{t_f}{2}\right]\frac{p_s}{2}-\frac{EAt_s(2+\beta t_0+(\overline{R}^2t_s/\beta{R_0}^2A))}{4\beta^3{R_0}^2A+4\beta^2\overline{R}^2t_s}\psi\right\} \tag{6}$$

Then substituting the expression of M from Eq. (6) into Eq. (1), the dynamic equation for the torsional vibration of the flange is obtained

$$\begin{aligned} \rho I_p\ddot{\psi}+\left[\frac{EI_r}{\overline{R}^2}+\frac{EAt_s(2+\beta t_0+(\overline{R}^2t_s/\beta{R_0}^2A))}{4\beta^3{R_0}^2A+4\beta^2\overline{R}^2t_s}\right]\psi &= \left[(R_1-R_0-r_c)-\frac{vR_0A(\beta t_0+1)}{2\beta^2{R_0}^2A+2\beta\overline{R}^2t_s}\right]p_t \\ -(R_1-R_f-r_c)(f_n\cos\alpha+f_f\sin\alpha)+\left[\frac{\overline{R}^2t_s(\beta t_0+1)}{2\beta^2{R_0}^2A+2\beta\overline{R}^2t_s}-\frac{t_f}{2}\right]\frac{p_s}{2} & \end{aligned} \tag{7}$$

Corresponding to the flange rotation angle ψ the axial displacement of the points on the middle surface of cylindrical shell is $z_r=\psi\Delta R$. By differentiating the expression of z_r with respect to time twice, the acceleration of the axial motion is given as $\ddot{z}_r=\ddot{\psi}\Delta R$. Substituting expressions of z_r and $\ddot{z}_r$ into Eq. (7) and introducing notations as follows for convenience of description:

$$m_r=\frac{\rho I_p}{\Delta R},\quad k_r=\frac{EI_r}{\overline{R}^2\Delta R}+\frac{EAt_s(2+\beta t_0+(\overline{R}^2t_s/\beta{R_0}^2A))}{4\beta^3{R_0}^2\Delta RA+4\beta^2\overline{R}^2\Delta Rt_s},\quad r_0=R_1-R_0-\frac{vR_0A(\beta t_0+1)}{2\beta^2{R_0}^2A+2\beta\overline{R}^2t_s},\quad t_r=\frac{\overline{R}^2t_s(\beta t_0+1)}{2\beta^2{R_0}^2A+2\beta\overline{R}^2t_s}.$$

The motion equation for axial vibration of the flange is

$$m_r\ddot{z}_r+k_rz_r=(r_0-r_c)p_t-(R_1-R_f-r_c)f_v+\left(t_r-\frac{t_f}{2}\right)\frac{p_s}{2} \tag{8}$$

2.3. Dynamic model for clamp band joint system

The clamp band joint system subjected to the axial vibration is shown in Fig. 4, where the axial displacement excitation z_H is acted on the bottom of lower interface ring and vibration is transmitted to the payload M through the clamp band joint. The payload mentioned here can be recognized as the spacecraft mounted on the launch vehicle. The model for calculating the payload response is shown in Fig. 5, where the mass of cylindrical shell is ignored since it is much small compared with the payload mass. $m=M/2\pi\overline{R}$ denotes the mass of payload in per unit length of circumference of the cylindrical shell at middle surface, where M is the payload mass, $k_s=k_s/2\pi\overline{R}$ denotes the axial stiffness of the cylindrical

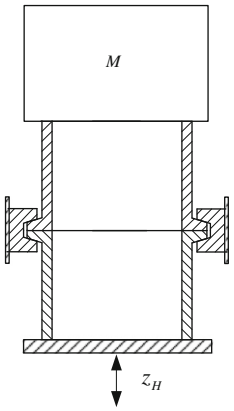

Fig. 4. Clamp band joint system under axial excitation.

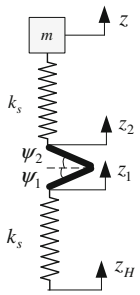

Fig. 5. Dynamic model for clamp band joint system.

shell in per unit length of circumference of middle surface, where $k_s=EA_s/l_s$ is the axial stiffness of cylindrical shell, A_s and l_s are the cross-section area and the length of the cylindrical shell, respectively.

The axial motion equation for the payload vibration can be easily obtained as

$$m\ddot{z}+k_s(z-z_2)=0 \tag{9}$$

where z is the axial displacement of the payload, z_2 is the axial displacement at the junction of the upper cylindrical shell and the flange. By defining that the positive direction of loads and displacements of the upper and lower flanges is symmetrical about the joint surface, z_2 can be expressed as

$$z_2=z_1+(\psi_1+\psi_2)\Delta R=z_1+z_{r1}+z_{r2} \tag{10}$$

where z_1 is the axial displacement at the junction between the lower cylindrical shell and the flange, ψ_1 and ψ_2 are the torsion angles of the lower and upper flanges, respectively, $z_{r1}=\psi_1\Delta R$ and $z_{r2}=\psi_2\Delta R$ are the relative axial displacements of the lower and upper flanges at the middle surface of the cylindrical shell about the joint surface, respectively. The axial motion equations for the lower and upper flanges are

$$\begin{aligned} m_r\ddot{z}_{r1}+k_rz_{r1}&=(r_0-r_c)p_{t1}-(R_1-R_f-r_c)f_{v1}+\left(t_r-\frac{t_f}{2}\right)p_{s1}\\ m_r\ddot{z}_{r2}+k_rz_{r2}&=(r_0-r_c)p_{t2}-(R_1-R_f-r_c)f_{v2}+\left(t_r-\frac{t_f}{2}\right)p_{s2} \end{aligned} \tag{11}$$

By analyzing the interactions of components of clamp band joint, the following relations can be obtained:

$$\begin{gathered} p_{t1}=k_s(z_1-z_H),\quad p_{t2}=k_s(z-z_2)\\ p_{t1}-f_{v1}=p_{t2}-f_{v2}\\ p_s=p_{s1}+p_{s2} \end{gathered} \tag{12}$$

According to assumption (5) proposed in Section 2.1, the upper and lower flanges vibrate symmetrically about the joint surface, then it can be obtained that $z_{r1}=z_{r2}=z_r$, $f_{v1}=f_{v2}=f_v$. By combining the motion equations for the lower and upper flanges together in Eq. (11) and then substituting Eqs. (10) and (12) into Eqs. (9) and (11), with simplification the dynamic

equations for the axial vibration of clamp band joint system are given by

$$\begin{aligned} m\ddot{z}+\frac{k_s}{2}z-k_s z_r &= \frac{k_s}{2}z_H \\ m_r\ddot{z}_r-\frac{k_s(r_0-r_c)}{2}z+(k_r+k_s r_0)z_r &= -\frac{k_s(r_0-r_c)}{2}z_H-(R_1-R_f-r_c)f_v+\left(t_r-\frac{t_f}{2}\right)\frac{p_s}{2} \end{aligned} \tag{13}$$

Here the axial vibration of clamp band joint system is considered as two degrees of freedom. In fact, the mass of the flange is also negligible compared with that of the payload. However, the inertial force item of the flange in Eq. (13) is vital for analyzing the dynamic characteristics at the joint surface and should not be ignored in the system motion equations.

It should be noted that the contact state between the interacting components varies as clamp band joint system vibrates. Consequently, model parameters f_n, f_f, R_f and r_c in the dynamic equations are not constants. Furthermore, the axial stiffness between the upper and lower interface rings will increase dramatically and restrict further axial compression as full contact is established between the interface rings during vibration. This unilateral constraint of axial deformation is not yet considered in Eqs. (8) and (13).

3. Identification of parameters in clamp band joint system model

3.1. Nonlinear finite element model for clamp band joint

In order to determine those unknown parameters in the dynamic model, a nonlinear finite element model of a cyclic section having one V-segment for the clamp band joint is developed using the ANSYS software as shown in Fig. 6, where face-to-face contact elements are applied between each contact pair. This model is nonlinear since the contact between joint components is considered. The baseline parameter values of the finite element model refer to a certain type of clamped joint interface of the LM-3A launch vehicle and are listed in Table 1, where μ is the friction coefficient between the interface ring and the V-segment. Unless otherwise stated, parameters may be assumed to have their baseline values.

Simulations are carried out statically on the model by applying loads in multiple steps: in the first load step the preload in the metal belts is generated by assigning the coefficient of thermal expansion to the metal belts and then applying virtual temperature variation, then an axial load cycle is applied on the interface rings by loading and unloading axial tension and then loading and unloading reversely axial pressure in sequence in the following next four load steps. And the cycle of axial loading is repeated until the stable state is achieved for the system.

3.2. Analysis of contact force distribution

As defined in Section 2.2, R_f and r_c are used to represent the distribution of the contact forces f_f and f_c, respectively, which are related to the structural parameters and the deformation of the interface rings. For a certain type of clamp band joint the structural parameters are definite. In this case, the deformation of the interface rings is determined by the magnitude of the preload and the axial load. Hence, only the effect of the preload and the axial load on the values of R_f and r_c is concerned here.

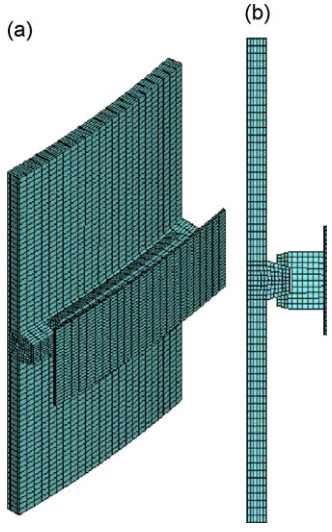

Fig. 6. Nonlinear finite element model for a cyclic section of the clamp band joint. (a) Finite element model for the clamp band joint and (b) cross section of the finite element model.

Table 1
Baseline parameter values for the clamp band joint model.

Symbol	Baseline value	Units
M	2300	kg
ρ	2700	kg/m^3
α	15	degree
R_1	0.6075	m
R_0	0.594	m
R_{f0}	0.6026	m
R_b	0.623	m
l_s	0.4	m
t_s	0.008	m
E	71.7	MPa
ν	0.33	
μ	0.125	

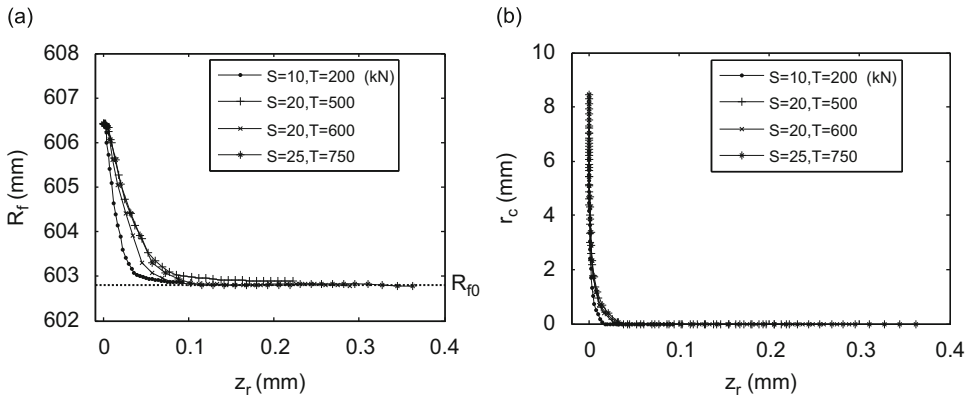

Fig. 7. Simulation results for different preloads and axial forces. (a) Variation of R_f with respect to z_r and (b) variation of r_c with respect to z_r.

Fig. 7 shows the variation of R_f and r_c in terms of axial displacement z_r for different combinations of preload and axial tension. The notation R_{f0} in Fig. 7(a) represents the radius at the point of the flange corresponding to the wedge head of the V-segment, which is illustrated in Fig. 2. Comparison of Fig. 7(a) and (b) indicates that the variation trends of R_f and r_c along with z_r are nearly the same. When z_r is relatively large, R_f is approximated to R_{f0}. At the same time, r_c is approximated to zero. It means that the contact forces f_f and f_c are focused at the points corresponding to the wedge head of V-segment and the outer edge of the flanges respectively. As z_r approaches to zero, the values of R_f and r_c increase rapidly to certain values. The increment of the values of R_f and r_c indicates that the acting points of the contact force resultants move away from the points where R_f=R_{f0} and r_c=0, respectively, when the relative axial displacement between the upper and lower flanges approaches to zero. At this moment the contact force f_c also suffers an obvious increment. This phenomenon is caused by the full contact of the upper and lower interface rings, which results in an axial constraint. The axial constraint can be represented by introducing an additional stiffness k_p in the motion equation for the axial vibration of the flange.

By considering the equation for the deformation of elastic compression and integrating the contact forces on the joint surface of the flanges, the contact stiffness k_p for the full contact between the upper and lower interface rings can be obtained

$$k_p = \frac{E(R_1-R_3)^3(R_1+3R_3)}{6t_0\overline{R}\Delta R} \tag{14}$$

Then the axial motion of the flange is divided into two states: when $z_r > 0$, the axial vibration of the flange is described by Eq. (8) deduced in Section 2.2; when $z_r \le 0$, the contact stiffness k_p between the upper and lower interface rings is added to k_r in the axial motion equation. Therefore, k_p can be expressed as

$$k_p = \begin{cases} 0, & z_r > 0 \\ \dfrac{E(R_1-R_3)^3(R_1+3R_3)}{6t_0\overline{R}\Delta R}, & z_r \le 0 \end{cases} \tag{15}$$

The value of this additional stiffness is much larger than that of the original stiffness k_r.

Since the abrupt increment of r_c is represented by adding k_p into the motion equation as z_r approaches to zero and the change of r_c can be neglected when z_r is relatively large, r_c=0 is adopted in the dynamic equations for the flange. As it can be seen in the following section that the magnitude of f_f becomes quite small as z_r approaches to zero, where the increment of R_f has little effect on the response of the joint system. Hence the variation of R_f is also neglected when z_r is small and it is assumed that R_f=R_{f0} in the dynamic equations.

3.3. Analysis of friction between flange and V-segment

Fig. 8 shows the variation of the axial displacement and the contact force between the flange and the V-segment during the cycle of axial loading for a preload S=25 kN and an axial load T=700 kN. It can be seen in Fig. 8 that the variation trends of the normal and tangential components of the contact force coincide. Around the points where the axial load reaches at the maximum tension and reverses its direction from tension to pressure the components of contact force change little with the variation of axial load, which indicates the occurrence of macro slip between the interface ring and the V-segment. When the axial load is in its pressure state, a full contact of the upper and lower interface rings takes place. At this moment the axial displacement remain constant and little relative motion between the interface ring and the V-segment occurs. Consequently, the tangential component of the contact force, that is, the friction force, approaches to zero as shown in Fig. 8.

Coulomb friction model is adopted to describe the friction force between the interface ring and the V-segment in terms of the axial displacement. Taking the full contact state into consideration, the friction force can be expressed by

$$f_f = \begin{cases} \mathrm{sgn}(\dot{z}_r)\mu f_n, & z_r > 0 \\ 0, & z_r \le 0 \end{cases} \tag{16}$$

Combining the equilibrium equation of the V-segment in radial direction and the expression of the axial component of the contact force between the interface ring and the V-segment

$$\begin{aligned} 2(f_n \sin\alpha - f_f \cos\alpha) &= p_s \\ f_v &= f_n \cos\alpha + f_f \sin\alpha \end{aligned} \tag{17}$$

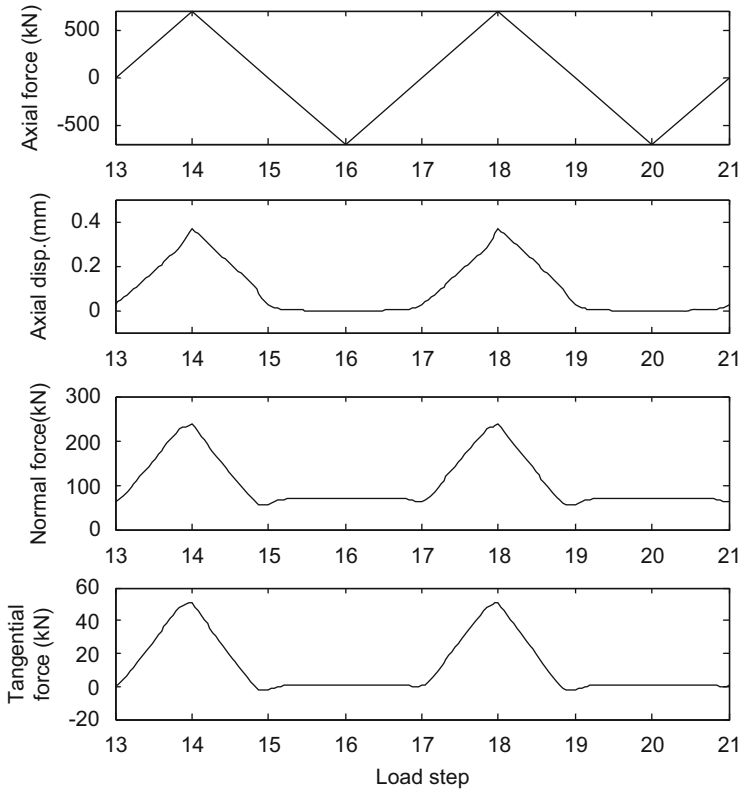

Fig. 8. Simulation results of the axial loading cycle for S=25 kN and T=500 kN.

and substituting f_f from Eq. (16) into Eq. (17), the axial component of contact force is given by

$$f_v = \begin{cases} \dfrac{\cos\alpha + \mathrm{sgn}(\dot{z}_r)\mu\sin\alpha}{2[\sin\alpha - \mathrm{sgn}(\dot{z}_r)\mu\cos\alpha]} p_s, & z_r > 0 \\ \dfrac{p_s}{2}\cot\alpha, & z_r \le 0 \end{cases} \tag{18}$$

To avoid numerical integration problems, the discontinuous friction force is smoothened using arc-tangent type function in the following simulations [13].

3.4. Dynamic model for clamp band joint system considering contact and frictional slippage

Based on the above analysis, the axial motion equation for the flange of the interface ring becomes

$$m_r\ddot{z}_r + (k_r + k_p)z_r = r_0 p_t - (R_1 - R_f)f_v + \left(t_r - \frac{t_f}{2}\right)\frac{p_s}{2} \tag{19}$$

Correspondingly, the dynamic equations for the clamp band joint system subjected to axial vibration are given by

$$\begin{aligned} m\ddot{z} + \frac{k_s}{2}z - k_s z_r &= \frac{k_s}{2}z_H \\ m_r\ddot{z}_r - \frac{k_s r_0}{2}z + (k_r + k_p + k_s r_0)z_r &= -\frac{k_s r_0}{2}z_H - (R_1 - R_{f0})f_v + \left(t_r - \frac{t_f}{2}\right)\frac{p_s}{2} \end{aligned} \tag{20}$$

where k_p and f_v are expressed in Eqs. (15) and (18), respectively. It is noted that no damping force is incorporated in Eq. (20). Actually, the joint system is subjected to not only the friction force but also other types of damping forces, such as structural damping force and environmental damping force. Hence, the damping ratio ξ=0.05 is adopted here. Then the equivalent damping of the dynamic system can be decided by

$$\begin{aligned} c &= \xi\sqrt{2k_s m} \\ c_r &= 2\xi\sqrt{(k_r + k_p + k_s r_0)m_r} \end{aligned} \tag{21}$$

By incorporating the equivalent damping into Eq. (20), the dynamic model for the clamp band joint system becomes

$$\begin{aligned} m\ddot{z} + c\dot{z} + \frac{k_s}{2}z - k_s z_r &= \frac{k_s}{2}z_H \\ m_r\ddot{z}_r + c_r\dot{z}_r - \frac{k_s r_0}{2}z + (k_r + k_p + k_s r_0)z_r &= -\frac{k_s r_0}{2}z_H - (R_1 - R_{f0})f_v + \left(t_r - \frac{t_f}{2}\right)\frac{p_s}{2} \end{aligned} \tag{22}$$

4. Experimental validation of the clamp band joint model

The effect of clamp band joint on the joint system is described by the axial motion equation for the flange of the interface ring, where the relationship between the relative axial displacements at the joint surface and the preload as well as the axial load is established. The inertial force in the motion equation is much small compared with the restoring force and the excitation forces. Hence, when investigating the clamp band joint locally, the inertial force can be neglected and the relative axial deformation at the joint surface can be obtained from Eq. (19)

$$Z_R = 2z_r = \frac{2r_0 p_t - 2(R_1 - R_f)f_v + (t_r - (t_f/2))p_s}{k_r + k_p} \tag{23}$$

Therefore, static experiments can be adopted to assess the validity of the clamp band joint model.

4.1. Experimental set-up

A test specimen, which is a 1:2.5 scale model of the finite element model developed in Section 3.1, is constructed based on the dimension theory. The configuration of the test specimen is similar to that of the clamp band joint illustrated in Fig. 1 except that only one metal belt is employed to fasten the V-segments and is tightened by a single bolt at the ends. Strain gauges are applied on the outer surface of the metal belt to measure the pretension in the metal belt and an extensometer is mounted on the inner surfaces of the interface rings across the joint surface to measure the relative axial displacement as shown in Fig. 9. The strain gauges and the extensometer are all calibrated in advance and mounted onto the test specimen when the belt is slack with no pretension applied.

The test specimen is mounted on a universal testing machine that is used to apply axial tension and pressure as shown in Fig. 10. Preload is applied to the metal belt through tightening the joint bolt. In order to achieve uniform belt tension the loading process is very slow and the belt is tapped successively around the periphery after each increment of loading until the anticipated preload is achieved. Then axial load is applied by the universal testing machine incrementally to the test specimen and the values of the relative displacement at the joint surface are recorded by the extensometer

Fig. 9. Configuration of the test specimen with the attachment of the extensometer.

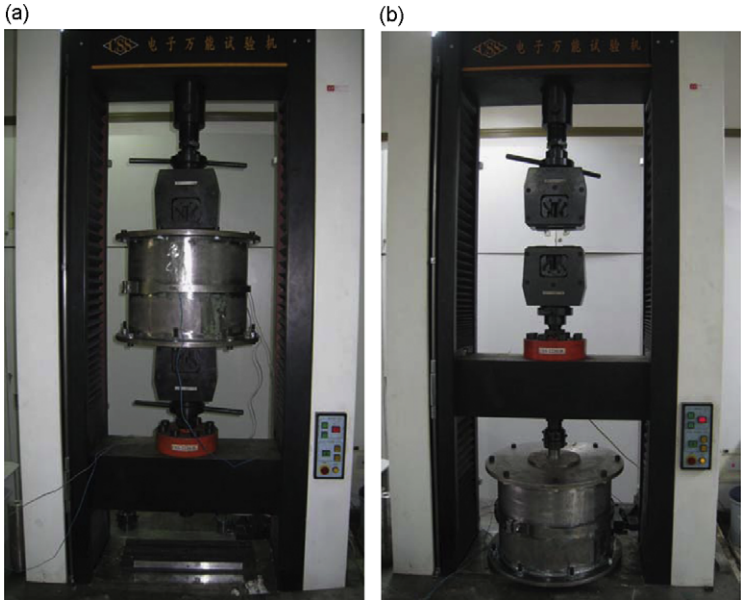

Fig. 10. Experimental set-up. Test specimen under (a) tension load and (b) pressure load.

correspondingly. It should be noted that the extensometer is reset before each cycle of the axial loading, which means that for each loading cycle the measured value of the initial relative displacement is zero.

4.2. Experimental results

The static experiments are carried out under different levels of preload. The relationships between the axial forces and the relative axial displacements under the preloads of 0.4 and 0.7 kN are shown in Fig. 11, where the maximum values of the axial load applied to the test specimen are 9 and 15 kN, respectively. In Fig. 11 the solid lines represent the analytical results that are obtained by substituting the structural parameter values of the test specimen and the values of the preload and axial load into Eq. (23).

It can be seen in Fig. 11 that the curve slope values of the analytical results are a little larger than those of the experimental results under the tension states, which means that the stiffness values of the analytical results are slightly large compared with those of the measured results. This difference is probably caused by the variation of the pretension in the metal belt during the axial loading process, which is assumed to be constant in the deduction of the dynamic model for the clamp band joint system. When the tension load is applied to the clamp band joint, radial compression of the flanges

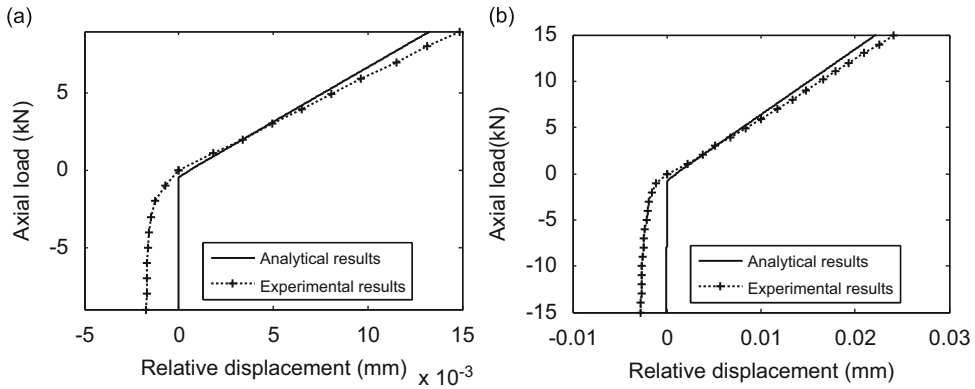

Fig. 11. Relation curves of axial force and relative axial displacement. (a) Relation curve for preload of 0.4 kN and (b) relative curve for preload of 0.7 kN.

takes place together with the torsional deformation, which will lead to the decrease of the pretension in the metal belt. Consequently, the decrement of the pretension affects the axial stiffness of the clamp band joint. However, the variation of the pretension is very small and its effect on the axial stiffness can be neglected. When the pressure load is applied to the test specimen, unreasonable negative relative displacements at the joint surface are observed in the experimental data as shown in Fig. 11. This phenomenon is due to the setup of the extensometer. The measured value of the extensometer is set to be zero at the beginning of each loading cycle as it is mentioned above. Whereas, the preload applied in the metal belt generates an initial gap between the upper and lower flanges before axial load acts. When the axial pressure load is applied the upper and lower flanges get into full contact. During this process the measured value of the extensometer changes from zero to a certain negative value that corresponds to the magnitude of the initial gap of the flanges. If the values of the initial gap are subtracted from the experimental results, the experimental results show good agreement with analytical ones.

It can be seen from the comparison that the calculated results give good correlation with the experimental data, thus the applicability of the clamp band joint model is validated.

5. Dynamic characteristics of clamp band joint system

5.1. Forced response of clamp band joint system subjected to axial excitation

The forced responses of the joint surface and the payload to a harmonic displacement excitation of amplitude Z_H=1 mm and different frequencies are shown in Fig. 12. It is revealed that the motions of the joint surface and the payload are often multiharmonic in nature. At a relatively low excitation frequency f_s=60 Hz, the motion has a second harmonic of the excitation frequency as shown in Fig. 12(a). As the excitation frequency is increased, sub-harmonic responses are typical as shown in Fig. 12(b) and (c), where $\frac{1}{2}$ sub-harmonic response can be observed. As the excitation frequency increases to 500 Hz, apart from the payload resonance frequency, no obvious multiharmonic response is found. This kind of behavior is common for nonlinear systems [14]. And as for the clamp band joint system, it is caused by the piecewise linear stiffness of the joint interface. Another phenomenon that should be noted is that as the excitation frequency increases the balance position of the payload moves upwards due to the opening of interface ring flanges.

In order to further investigate the effect of the clamp band joint on the dynamic characteristics of the jointed system, the model shown in Fig. 4 is reconsidered by removing the clamp band joint and fixing the upper and lower interface rings together. In this case there will be no relative displacement at the joint surface. Then the model is simplified to a linear system of single degree of freedom with motion equation given by

$$m\ddot{z}+c\dot{z}+\frac{k_s}{2}z=\frac{k_s}{2}z_H \tag{24}$$

Response amplitudes of the payload with and without clamp band joint for different excitation frequencies and a constant amplitude of $|z_H|$=1 mm are shown in Fig. 13. Those two frequency–response curves illustrate the transfer characteristics of the joint system and the corresponding linear system. It can be seen from Fig. 13 that the resonance frequency of the linear system with the interface rings fixed together is 242 Hz. Whereas the primary resonance frequency of the clamp band joint system displays a deviation away from that of the corresponding linear system and changes to be 130 Hz. The decrement of the resonance frequency results from the decrease of the system stiffness that is caused by the presence of clamp band joint. Besides, there exist relatively large amplitudes of components near 66 and 254 Hz in the frequency–response curve of the clamp band joint system. Jump phenomenon is also observed around frequencies of 412 and 463 Hz, which are illustrated by dashed lines in Fig. 13. The nonlinear characteristics observed in the responses of the joint system are induced by the piecewise linear stiffness resulting from the clamp band joint, which brings the asymmetric constraint of axial deformation and the frictional contact into the clamp band joint system.

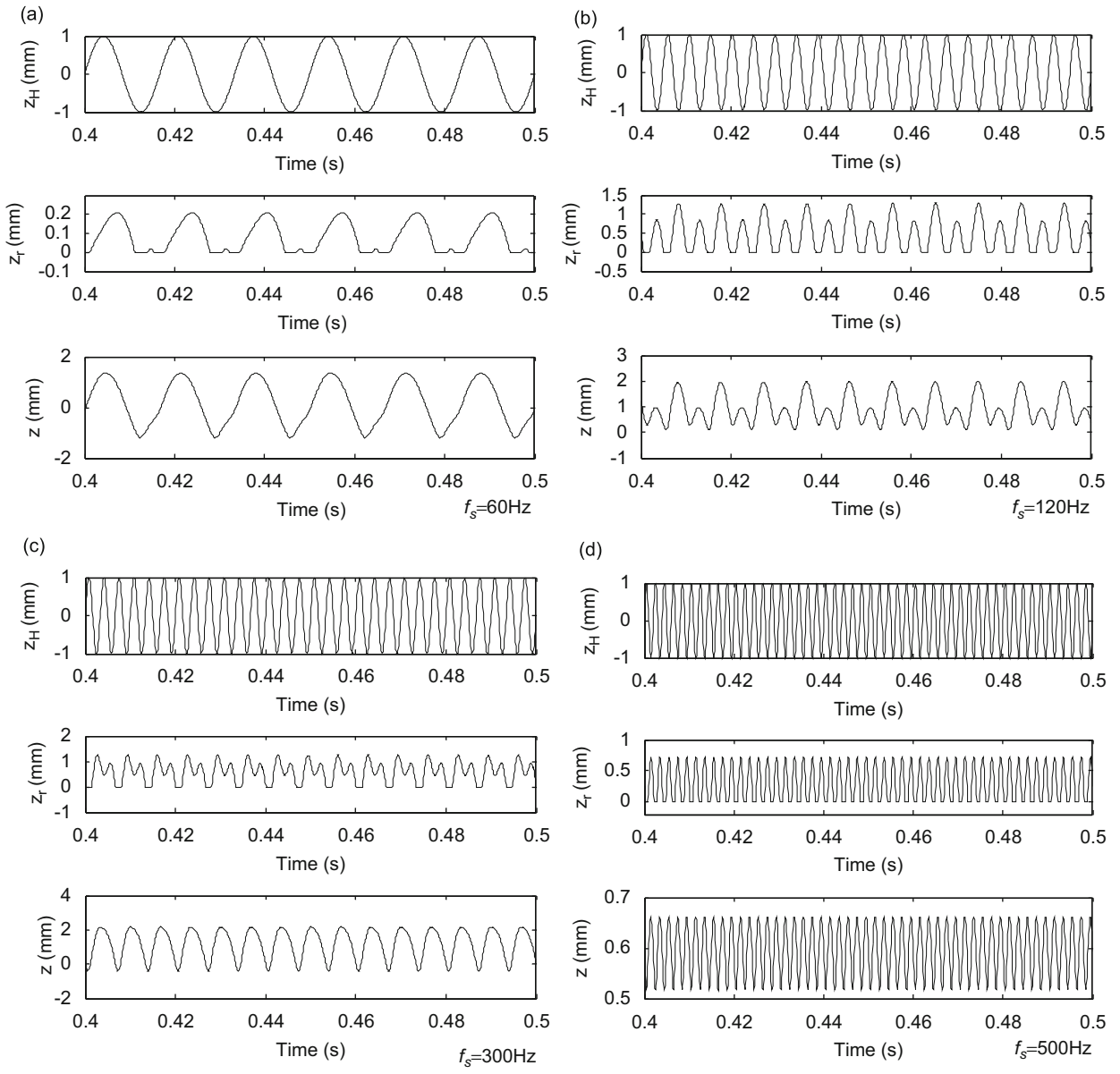

Fig. 12. Joint surface and payload responses for different excitation frequency. Response for excitation of (a) f_s=60 Hz, (b) f_s=120 Hz, (c) f_s=300 Hz and (d) f_s=500 Hz.

The jumping behavior can be clearly seen in time domain by frequency sweeping across the jump point. Taking the jump around 463 Hz as an example, the time response of the payload is shown in Fig. 14. It can be seen in Fig. 14 that the axial displacement of the payload in the first 0.2 s reaches the amplitude at the upper branch of the frequency–response curve for the excitation frequency of 462.8 Hz. Then the response amplitude jumps to the lower branch after a transient period as the excitation frequency is perturbed to 462.9 Hz. And when the excitation frequency returns to 462.8 Hz, the response amplitude still stays at the lower branch.

5.2. The effect of wedge angle on response of clamp band joint system

The wedge angle α of the flanges is an important parameter for the clamp band joint. As for the clamp band used to connect pipes, α is usually designed to be small enough to realize the self-lock between the interface ring and the V-segment, which makes the connection more reliable. However, when used in the aerospace industry, separation of the upper and lower interface rings should be concerned and no self-lock is allowed. Thus α must be chosen properly to meet the requirements for both joint and separation.

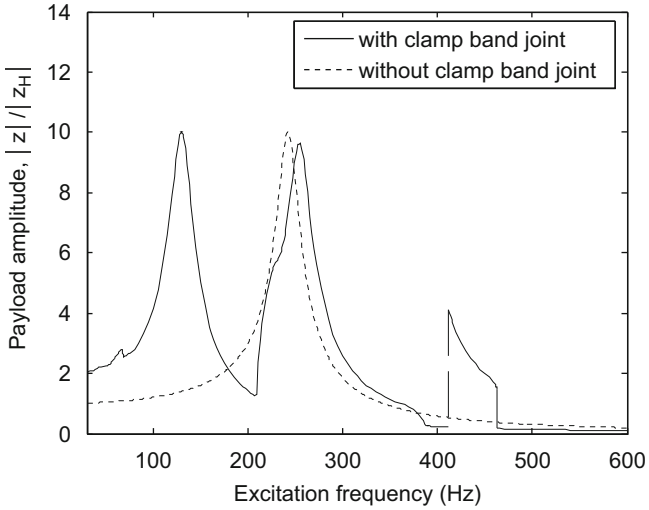

Fig. 13. Frequency–response curves with and without clamp band joint. Primary resonance frequency of the clamp band joint system: 130 Hz; resonance frequency of the corresponding linear system: 242 Hz.

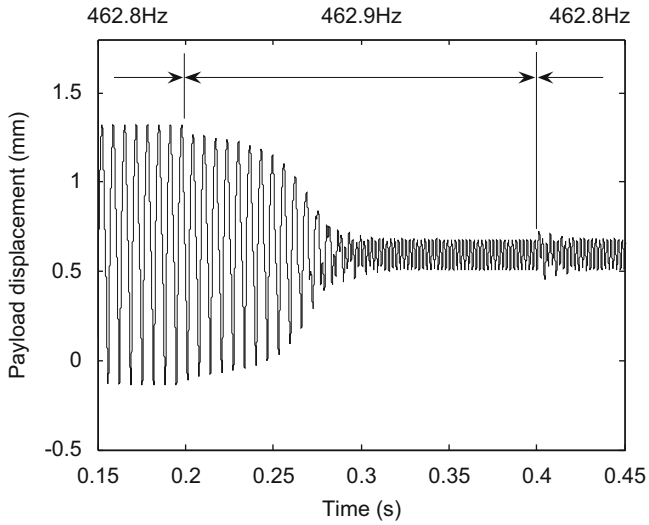

Fig. 14. Time simulation of the jump phenomenon.

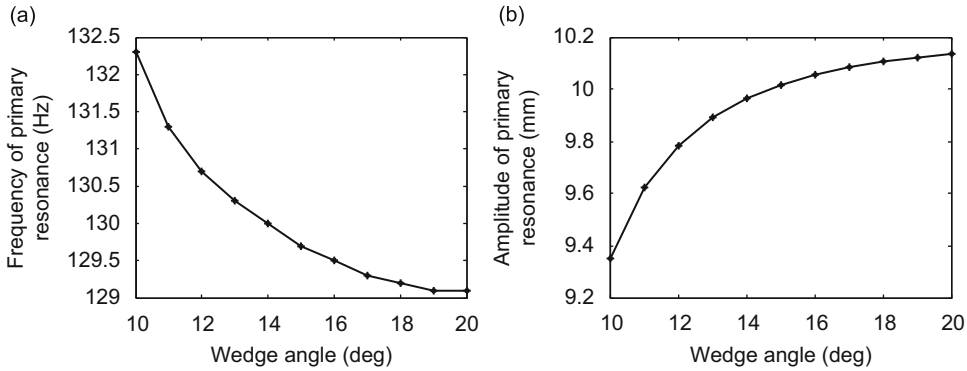

Fig. 15. Variation of the primary resonance response of the payload for different values of the wedge angle. (a) Variation of frequency with respect to wedge angle and (b) variation of amplitude with respect to wedge angle.

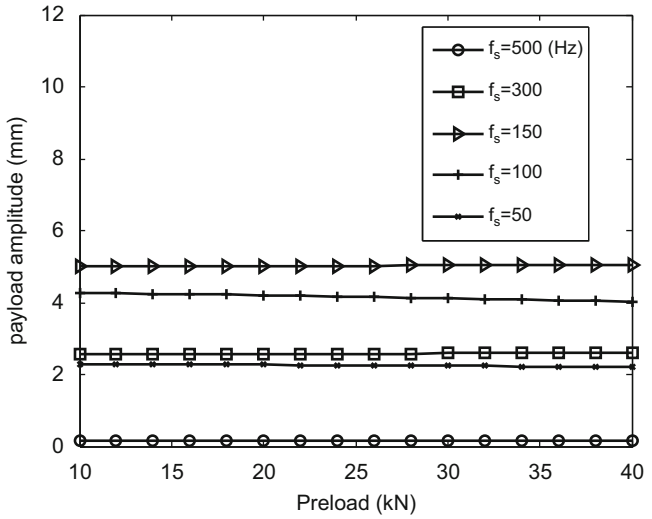

Fig. 16. Variation of response amplitude of the payload with respect to preload for different excitation frequencies.

The maximum value of α that may lead to self-lock is 7.1° according to the baseline value of the friction coefficient μ listed in Table 1. Then the variation of α is set from 10° to 20°. The variations of the frequency and amplitude of the payload primary resonance response in terms of the wedge angle are shown in Fig. 15. From these curves it can be seen that the resonance frequency of the payload decreases as the wedge angle is increased. In the meantime the resonance amplitude increases. And as the wedge angle increases the change rates of frequency and amplitude become smaller. The increment of the wedge angle weakens the constraint effect of the preload on the interface rings transferred through the wedging action, which results in the decrease of the clamp band joint stiffness and consequently changes the resonance frequency and amplitude of the payload.

It should be noted that the variation of the wedge angle is restricted in a small range for analyzing its effect on the system response, since large variation of the structural parameters might lead to the invalidity of the assumptions and approximations made in this paper. In that case, the dynamic equations derived here could not represent the dynamic characteristics of the clamp band joint. For instance, considering the limit case of zero wedge angle, it is obvious that the relative deformation between the flanges and the V-segments and the contact force distribution would be significantly different from those under the baseline value of the wedge angle listed in Table 1. In this case the approximation for R_f and r_c made in Section 3.2 will lead to incorrect results and cannot be used any more.

5.3. The effect of preload on response of clamp band joint system

The effect of preload on the response amplitude of payload is also investigated. Fig. 16 shows the relationship between the amplitude of the payload and the preload for different excitation frequencies. It can be seen from Fig. 16 that there is no obvious change in the response amplitude as the magnitude of the preload is increased from 10 to 40 kN, which indicates that the response amplitude is insensitive to the variation of the preload. This simulation result coincides with the analysis result reported in Ref. [10], where it was verified that although the increase of the preload could improve the allowable clamp design load, the variation of the preload in certain range had little effect on the joint stiffness when the applied axial load was within the range of the allowable load.

6. Conclusions

The dynamic model of the clamp band joint system subjected to axial excitation has been developed on the basis of the axial dynamic equation for the flange of the interface ring jointed by clamp band. In the model, the contact and frictional slippage between the components were accommodated. Some model parameters that vary along with the axial deformation of the joint system were determined by nonlinear finite element analysis. A 1:2.5 scale model of the clamp band joint was constructed and static experiments were carried out to validate the clamp band joint model. The dynamic model was then used to study the forced response of the clamp band joint system to axial excitation and the nonlinearity caused by the clamp band joint. The effects of the wedge angle of the clamp band joint and the magnitude of the preload on the responses were also discussed.

The calculated results based on the joint model showed good agreement with the experimental data, therefore the validity of the presented joint model was verified. Simulations on the proposed dynamic model for the clamp band joint system revealed that the clamp band joint reduced the system stiffness and brought nonlinearity to the system, where

multiharmonic responses occurred in the responses of the joint surface and the payload to harmonic excitation. Jump phenomenon of the payload response was also observed due to the discontinuity of the system stiffness. Parameter studies indicated that an increase of the wedge angle led to the decrease of the resonance frequency and the increase of the resonance amplitude of the payload. Besides, variation of the preload had no obvious effect on the system response as the excitation stayed within the allowable clamp design load.

References

[1] I_Shih Chang, Investigation of space launch vehicle catastrophic failures, *Journal of Spacecraft and Rockets* 33 (2) (1996) 198–205.
[2] C.S. Lin, T.R. Cole, Dynamic model for global positioning system block IIR space vehicle, *Journal of Spacecraft and Rockets* 34 (3) (1997) 354–359.
[3] A.A. Ferri, Modeling and analysis of nonlinear sleeve joints of large space structures, *Journal of Spacecraft and Rockets* 25 (5) (1988) 354–360.
[4] L. Gaul, J. Lenz, Nonlinear dynamics of structures assembled by bolted joints, *Acta Mechanica* 125 (1997) 160–181.
[5] Y. Song, et al., Simulation of dynamics of beam structures with bolted joints using adjusted Iwan beam elements, *Journal of Sound and Vibration* 273 (2004) 249–276.
[6] A.D. Crocombe, R. Wang, G. Richardson, C.I. Underwood, Estimating the energy dissipated in a bolted spacecraft at resonance, *Computers and Structures* 84 (2006) 340–350.
[7] D.T. Robert, E. Michael, Nonlinear finite element evaluation of marman clamp structural capability, *AIAA/ASME/ASCE/AHS/ASC Structures, Structural Dynamics and Materials Conference* 1 (1994) 320–330.
[8] K. Shoghi, H.V. Rao, S.M. Barrans, Stress in a flat section band clamp, *Proceedings of the Institution of Mechanical Engineers, Part C: Journal of Mechanical Engineering Science* 217 (7) (2003) 821–830.
[9] K. Shoghi, H.V. Rao, S.M. Barrans, Stress in V-section band clamps, *Proceedings of the Institution of Mechanical Engineers, Part C: Journal of Mechanical Engineering Science* 218 (3) (2004) 251–262.
[10] Z.Y. Qin, S.Z. Yan, F.L. Chu, Axial stiffness analysis of clamp band system, *Journal of Astronautics* 30 (5) (2009) 2080–2085 (in Chinese).
[11] Marman clamp system design guidelines, Guideline No. GD-ED-2214, NASA Goddard Space Flight Centre 2000.
[12] S. Timoshenko, S. Woinowsky-Krieger, *Theory of Plates and Shells*, McGraw-Hill Book Co., Inc., New York, 1985 429–465.
[13] T.C. Kim, T.E. Rook, R. Singh, Effect of smoothening functions on the frequency response of an oscillator with clearance non-linearity, *Journal of Sound and Vibration* 263 (2003) 665–678.
[14] C. Hayashi, *Nonlinear Oscillations in Physical Systems*, McGraw-Hill Book Co., Inc., New York, 1964 128–180.